

# Adamantane-based low-dielectric-constant photocurable resin for 3D printing electronics

Jhu-Lin You<sup>a,c</sup>, I.-Tseng Liu<sup>b</sup>, Yu-Ho Chen<sup>a</sup>, Ramachandran Balaji<sup>d</sup>, Shih-Huang Tung<sup>a,\*</sup>, Ying-Chih Liao<sup>b,\*</sup>

<sup>a</sup> Institute of Polymer Science and Engineering, National Taiwan University, Taipei 10617, Taiwan

<sup>b</sup> Department of Chemical Engineering, National Taiwan University, Taipei 10617, Taiwan

<sup>c</sup> Department of Chemical & Materials Engineering, Chung Cheng Institute of Technology, National Defense University, Taoyuan 335, Taiwan

<sup>d</sup> Department of Electronics and Communication Engineering, Koneru Lakshmaiah Education Foundation, Andhra Pradesh 522302, India

## ARTICLE INFO

### Keywords:

Low dielectric constants  
3D printing, Photocurable  
Acrylic-polyurethane  
Adamantane  
Electroless plating

## ABSTRACT

In this work, a novel formulation is developed to prepare photocurable polyurethane acrylate (PUA) resin with a low dielectric constant for 3D printing applications. To amend the deficient electronic properties of regular 3D printed PUA materials, a symmetric polymer structure 1,3-adamantanediol (ADO) is introduced into the PUA polymer matrix to effectively decrease the dielectric constant. A low dielectric constant ( $D_k = 2.26$ ) and a low loss tangent ( $D_f = 0.018$ ) at 10 GHz after formulation, are significantly lower than commercial PCB materials (High Tg FR-4,  $D_k = 4$  and  $D_f = 0.02$ ). The modified PUA also exhibits great mechanical properties (tensile strength 12.02 MPa and elongation break at 111.35%) and can be further metalized with adhesive copper layers (5B adhesion test). With little addition of BN powder (1 wt%), the  $D_f$  of PUA resin can also be effectively reduced ( $D_f = 0.006$ ), and the measured values of its metalized substrate antenna parameters are proven to be within the acceptable range for 5 G devices. The PUA resin can also be printed into complex 3D structures for 5 G flexible circuit board applications with good design flexibility, and the low dielectric constant provides the opportunity to replace traditional rigid FR-4 substrates for 5 G flexible board applications.

## 1. Introduction

High-performance millimeter wave (mmWave) modules have attracted significant attention in recent years due to the growing demands in electronic signal transmission at higher frequencies, especially for the fifth-generation mobile communications technology (5 G technology). As chip sizes continue to shrink, polymers with low dielectric constant (low-k material:  $D_k \leq 2.5$ ) play an important role in chip packaging. Additionally, as current chip packaging designs continue to evolve, the demand for 3D objects is growing rapidly. These polymers serve as the insulating materials to reduce signal delay and maintain signal authenticity. Polyimide (PI), liquid crystal polymer (LCP), and polytetrafluoroethylene (PTFE) are famous for their low  $D_k$  and thus are commonly used in chip packaging applications. Despite the good dielectric properties, these polymers are mostly used in the form of thin films or circuit board substrates due to the limitations on their inherent mechanical or rheological properties, making them unsuitable for 3D object fabrication. To meet these demands, there is a pressing need to

develop polymer materials that possess both low  $D_k$  and 3D-printing capabilities. Such advancements have the potential to revolutionize the production of next-generation electronics, offering enhanced flexibility and efficiency for electronic devices in the 5 G era.

Photocurable 3D printing technology is a widely used fabrication method for complex and customized products due to its high printing precision, low cost, and good repeatability [1,2]. Among various photocurable resins for 3D printing technology, polyurethane acrylate (PUA) is commonly used because of its flexibility, miscibility, compatibility, and simple film-forming behavior [3–5]. With a polyurethane (PU) backbone, the mechanical and chemical properties of PUA can be adjusted by altering the proportion of hard (rigid) and soft (flexible) chain segments (NCO/OH component, or so-called R-value) [6,7]. Polyurethanes with different R-values are composed of different numbers of urethane segments, leading to varying numbers of hydrogen bonds formed between molecular chains. These differences indirectly affect the dielectric properties due to variations in polarity. Importantly, the R-value has a significant impact on the molecular weight of PUA

\* Corresponding authors.

E-mail addresses: [shung@ntu.edu.tw](mailto:shung@ntu.edu.tw) (S.-H. Tung), [liao@ntu.edu.tw](mailto:liao@ntu.edu.tw) (Y.-C. Liao).

<https://doi.org/10.1016/j.addma.2024.104047>

Received 29 September 2023; Received in revised form 21 January 2024; Accepted 13 February 2024

Available online 17 February 2024

2214-8604/© 2024 Elsevier B.V. All rights reserved.

resin, which is related to the quality of 3D photo-curing printing. Hence, the selection of an appropriate R-value is crucial for achieving the desired quality of the low-dielectric 3D photocurable resin. In addition, the surface energy of PUA can be easily enhanced through chemical etching or plasma to provide good adhesion strength for electrodepositing metal layers. However, the Dk and Df of PUA are still too high for 5 G electronic applications [8–10]. To reduce the Dk of polymer materials, a commonly used method is to introduce either porous material [11–13] or inorganic dielectric fillers in polymer matrices [14–17]. The porous structures are susceptible to water absorption, and thus seriously affect the mechanical stability of the composite materials [18–20]. In contrast, the addition of inorganic dielectric fillers in a polymer matrix can largely improve the composite dielectric properties without water absorption problem, but the filler selection remains challenging. Besides, there are many complicated factors that affect Df, including polarization characteristics and molecular stacking. To reduce the Df of polymer materials, so far, mixing inorganic dielectric fillers in a polymer matrix is still the most common method for fabricating low-loss dielectric materials. Several investigations on the use of Boron nitride (BN) as a low-loss dielectric have been reported, showing promising results [21,22]. Compared with other fillers, such as SiOF, Al<sub>2</sub>O<sub>3</sub>, and AlN, BN not only has a range of advantages such as low dielectric constant (Dk < 3.9) and low dielectric loss (Df < 0.001), but also has good thermal conductivity (420 W/mK).

On the other hand, the introduction of low polarizability branch structures into the PUA polymer backbone provides an alternative approach for Dk reduction [23–26]. The structural design of PUA is the fundamental solution to the Dk reduction without sacrificing processibility. Inserting a symmetric three-dimensional chemical structure, such as adamantane (AD), creates the possibility for Dk reduction. AD is a hydrocarbon with a bulky three-dimensional structure, comprising three fused chair-form cyclohexane rings, which exhibit high stiffness, stable thermal properties, high density, and antioxidant properties [27]. This structure effectively increases the free volume (V<sub>f</sub>) throughout the polymer matrix and reduces the Dk [28]. Recent studies have shown the possibility of incorporating the adamantane group into polymer backbones to enhance the intrinsic properties of the polymer matrix [29–31] for dental and other applications. However, the feasibility of AD-containing polyurethane resins for 3D printing technology has not been studied. Therefore, here we propose to introduce 1,3-adamantanediol (ADO) into the backbone of photocurable PUA to increase the V<sub>f</sub> of the entire polymer chain, thereby reducing the Dk. At the same time, in order to obtain a more desirable dielectric material, we attempted to reduce the higher Df caused by the inherent properties of polyurethane-based materials by blending a small amount of Boron Nitride fillers (Platelets CFP 006 purchased from 3 M Science. Applied to Life. TM) into the resin.

In this study, we propose a novel strategy to synthesize a low Dk photocurable resin, specifically designed for 3D printing technology, leveraging the unique properties of adamantane. To achieve a markedly reduced Dk, along with the benefits of high thermal stability and exceptional mechanical properties, a rigidly symmetric and nonpolar chemical structure, ADO, is selected. The effects of different PUA formulations and ADO ratios in the PUA resins as well as a small amount of BN blending are investigated to optimize the dielectric properties of the ADO-incorporated UV-curable resins. The mechanical properties, thermal stability, and metal layer adhesion of the resin are tested to evaluate its applicability for 5 G electronics and to compare its performance with commercial PCB materials (High Tg FR-4). This low-k resin has potential applications as an alternative to rigid FR-4 substrates in bendable circuit boards, flexible 3D architectures, insulating layers for semiconductor devices, and many other high-frequency applications.

## 2. Material and methods

### 2.1. Materials

Dicyclohexylmethane 4,4'-diisocyanate (H<sub>12</sub>MDI, purity > 99.0%), poly(tetrahydrofuran) (PTMEG, average M<sub>n</sub> = 650 g/mol), 1,3-adamantanediol (ADO, purity > 99.0%), poly(dimethylsiloxane) (PDMS hydroxy-terminated, average M<sub>n</sub> = 550 g/mol), di-n-butyltindilaurate (DBTDL, purity > 95.0%), 2-hydroxyethyl acrylate (2-HEA, purity > 96.5%), and acetone (purity > 99.9%, solvent) were purchased from Sigma-Aldrich, USA. The cross-linker, trimethylolpropanetri-acrylate (TMPTA), and photo-initiator (2,4,6-trimethyl benzoyl)-diphenylphosphine oxide (TPO) were purchased from Double Bond Chemical Ind., Co., Ltd, Taiwan, and used as received. To prevent moisture from affecting the synthesis reaction, PTMEG and ADO were dried in a vacuum at 85 °C for 5 h before use.

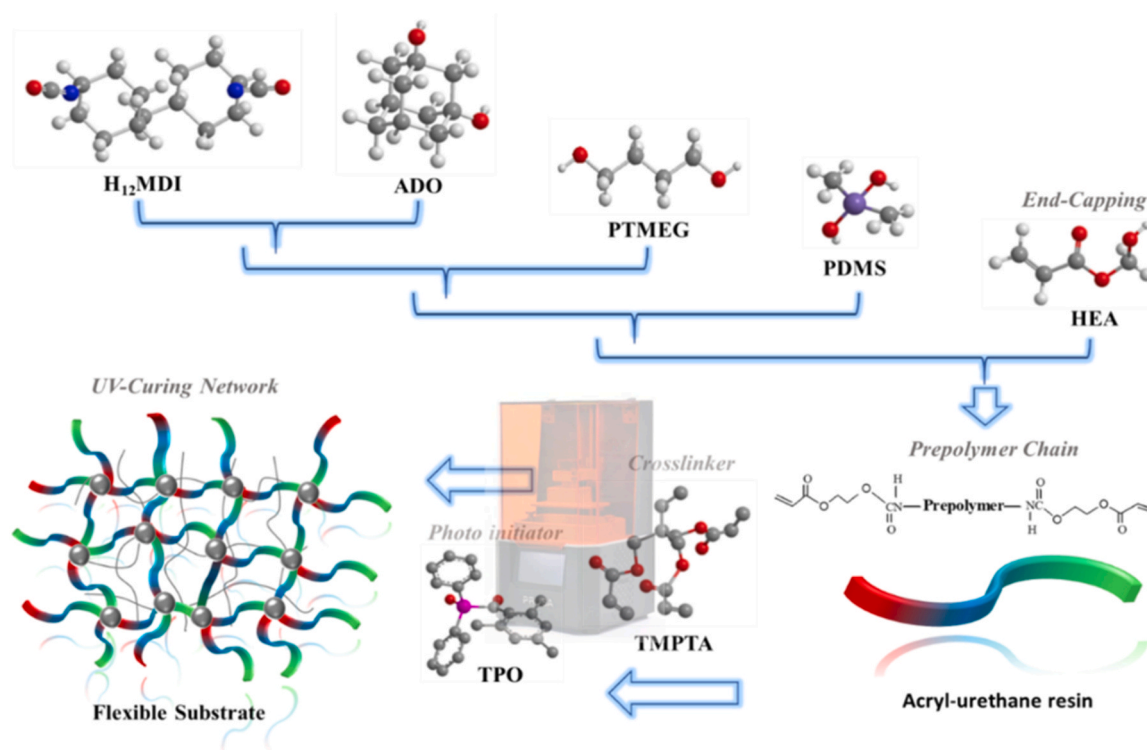
### 2.2. Synthesis of polyurethane-acrylate (PUA) resin formulation

The PUA resin is composed of 4,4'-methylene dicyclohexyl diisocyanate (H<sub>12</sub>MDI) as the isocyanate, poly(tetrahydrofuran) (PTMEG), PDMS hydroxy-terminated, and 1,3-Adamantanediol (ADO) as the polyol, and 2-hydroxyethyl acrylate (2-HEA) as an acrylate. Scheme 1. presents the synthesis process of the resins and the LCD 3D printing process. In the first step of the condensation polymerization, ADO was added to a 250 mL three-necked round bottom flask equipped with a reflux condenser, a dropping funnel, a mechanical stirrer, and a thermometer under a nitrogen atmosphere. H<sub>12</sub>MDI and DBTDL were dropped slowly into the flask and stirred at 80 °C for 2 hours. Later, PTMEG was added to the above mixture, followed by stirring at 80 °C for 3 hours. Then, PDMS was slowly added to the reactor to form a PU prepolymer at 60 °C for 2 hours. Finally, the end-capping agent 2-HEA was added slowly into the flask and which reacts with the PU prepolymer to cap the terminal NCO groups. Acetone was carefully added to reduce the viscosity of the PU prepolymer throughout the synthetic process. In the reaction steps, Fourier transform infrared (FTIR, Thermo Fisher Scientific, Nicolet iS5, Sweden) spectra of the synthesized PUA resins were obtained at a resolution of 4 cm<sup>-1</sup> with 32 scans over the spectral range from 400 to 4000 cm<sup>-1</sup>. Given the effect of molecular weight on the property of the PUA resin, an optimized R-value can be a pivotal factor affecting UV-curing behavior during the LCD 3D-printing process. Thus, a series of PUA resin formulations with different R values were synthesized for the sake of understanding the influence of the R values on the molecular weight of PUA resins. The R-value was calculated by the following equation [32]:

$$R \text{ value} = \frac{NCO}{OH} = \frac{H_{12}MDI}{ADO + PTMEG + PDMS}$$

### 2.3. Preparation of formulations for 3D LCD-printing

An LCD 3D printer (Sonic Mini 4 K, PHROZEN TECH CO., LTD. Taiwan), equipped with a resolution of 3840 × 2160 UHD (722 PPI), a 120 × 60 mm LCD screen, a 405 nm wavelength UV-LED source and a vertically-movable metal platform (shortest moving distance of 35 μm), was used for sample fabrication. A UV-curable resin mixture consisted of 95 wt% PUA resin and 5 wt% TMPTA was prepared by strong stirring under room temperature. Then, 4 wt% TPO was added based on the total weight of the UV-curable resin. As illustrated in Scheme 1, in the LCD 3D-printing procedure, the thickness of each printed layer was set to be 50 μm with an exposure time of 100 seconds. The 3D-printed samples were then post-cured for 10 minutes to ensure the absence of resin residue on their surfaces [33].



**Scheme 1.** Synthetic routes of polyurethane-acrylate (PUA) resins and the crosslinking mechanism for the LCD 3D-printing process with tri-functional monomer (TMPTA), and photo-initiator (TPO).

#### 2.4. Electroless plating

The surface metallization of the printed sample was performed using the following steps. First, to activate the printed sample surface, a plasma activation was performed in a plasma chamber (Henniker plasma, HPT-100, UK) at 150 W for 20 minutes with an oxygen flow rate of 10 standard cubic centimeters per minute (sccm). Next, the Pd nanocatalyst reported in previous studies [34,35] was dip-coated on the plasma-treated sample and dried in an oven at 90 °C for 15 minutes. Finally, the Pd-catalyst-covered sample was immersed in an electroless bath for copper deposition. More details for the electroless copper bath and process conditions can be found in the previous work [34,35]. The average thickness of the Cu layer of the metallized substrate was determined by XRF analysis (Bowman, B Series, US).

#### 2.5. Characterization

<sup>1</sup>H NMR analysis of the structure of PUA resin was carried out with a (Bruker, AVANCE III HD 600 MHz, US) spectrometer, operating with sample solutions of CDCl<sub>3</sub>. Chemical shifts were given in the  $\delta$  scale in parts per million (ppm). The polydispersity (PDI) and molecular weight (M<sub>n</sub> and M<sub>w</sub>) of the synthesized PUA resins were analyzed using gel permeation chromatography (GPC) on a Waters GPC instrument equipped with a UV and refractive index (RI) detector; the column was calibrated using polystyrene standards with a narrow molar mass distribution. Dimethylformamide was utilized as a solvent and applied at a flow rate of 1.0 mL min<sup>-1</sup> with a sample concentration of 1 mg mL<sup>-1</sup>. The dielectric properties (D<sub>k</sub> and D<sub>f</sub>) of the printed substrates were measured by a vector network analyzer (Rohde & Schwarz, ZNB20, Germany) at 10 GHz under room temperature (25 °C). The thermal stability of printed substrates was determined by TGA (Mettler, TGA-2 SF, Switzerland) at a ramp rate of 10 °C min<sup>-1</sup> under a nitrogen environment from 100 to 600 °C. The mechanical properties were evaluated by using a universal material test machine (CT, QC-526M1F, Taiwan). The tensile test speed was 10 mm min<sup>-1</sup> with dumbbell-shaped

specimens (50 mm × 5 mm × 0.8 mm). Dynamic mechanical analysis (DMA) of these substrates was performed using DMA tester (TA, DMA 850, US) at 1 Hz scanning with a 5  $\mu$ m amplitude over the temperature range of -70 to 70 °C at 3 °C min<sup>-1</sup>. The coefficient of thermal expansion values was obtained using a thermomechanical analyzer Q400EM from TA Instruments. The TMA spectra of the sample were obtained in the heating and cooling states at a rate of 3 °C min<sup>-1</sup> in the temperature range of -90 to 90 °C. The linear coefficients of thermal expansion, denoted as  $\alpha_1$  and  $\alpha_2$ , and glass transition temperature (T<sub>g</sub>) for each sample were calculated in specific regions both below and above the phase transition using the linear regression least square method. The soluble fraction (unconnected to the network) was extracted using Soxhlet extraction by exposure to refluxing boiling xylene solvent for 10 hours, while the cross-linked structure was the insoluble part. These fractions are calculated as follows: Gel fraction = W (the weight of the remaining after filtered and dried) / W<sub>0</sub> (the initial weight of the sample).

### 3. Results and discussion

#### 3.1. Synthesis and characterization of ADO-PUA resin

The chemical structures of synthesized polyurethane-acrylate (PUA) resins are first examined by using FT-IR spectroscopy, as shown in Fig. 1. Table 1 lists the experimental molar formulations of the ADO-PUA resins used in the study. The condensation reaction between NCO and hydroxyl (OH) groups leads to gradual peak decrease at 2250 cm<sup>-1</sup>, the fingerprint of NCO group. Isocyanate (NCO) stretching vibrations are monitored at each step with various reaction time. Meanwhile, the formation of urethane group (NHCOO) results in the concomitant appearance of the stretching N-H bonds at 3280–3400 cm<sup>-1</sup>, the bending vibrations of N-H bonds at 1520–1550 cm<sup>-1</sup>, and the stretching vibration peak of C=O at 1735–1750 cm<sup>-1</sup>. Moreover, due to the intermolecular hydrogen bonding of macromonomer (prepolymer) segments formed after the addition of PTMEG and PDMS, a small shift in the N-H

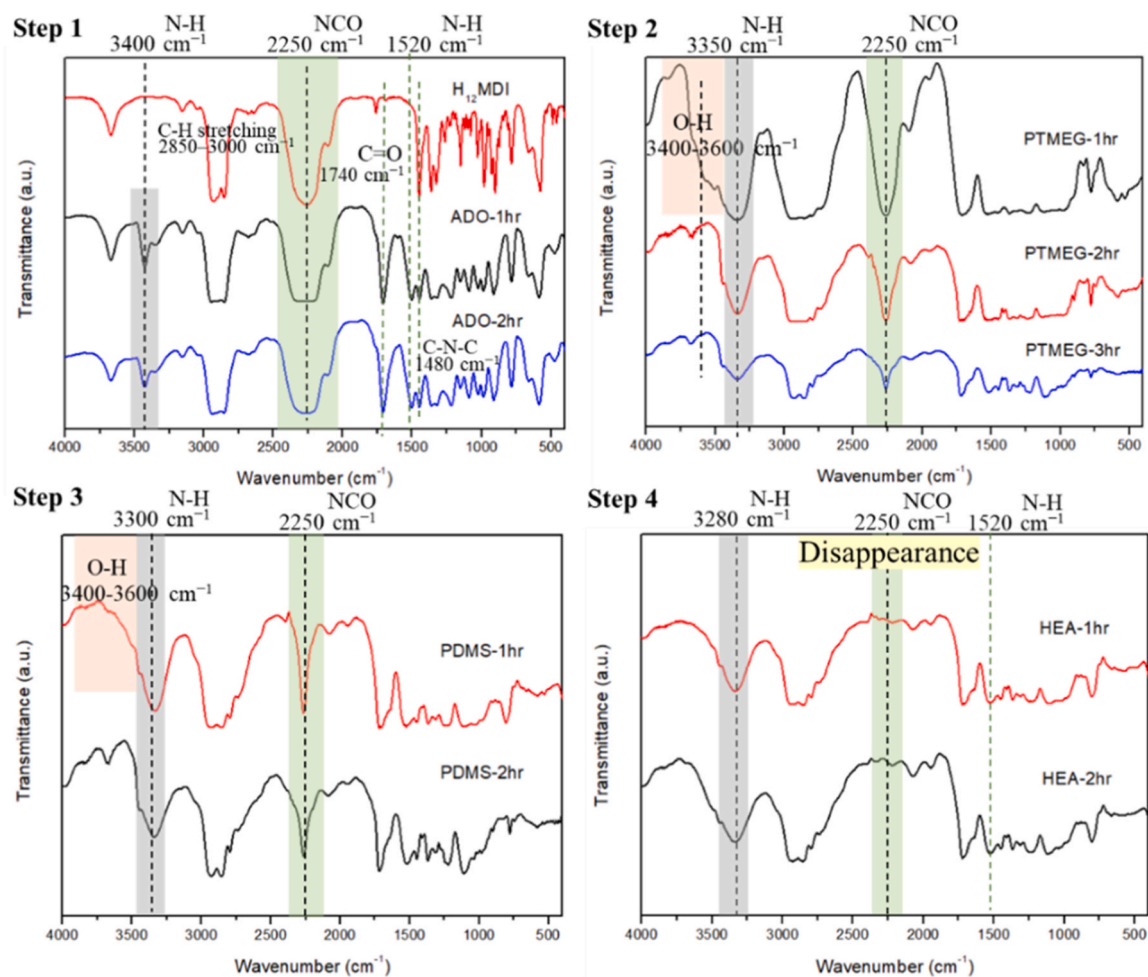


Fig. 1. FT-IR spectrum of the synthesized polyurethane-acrylate (PUA) resin.

Table 1

The experimental molar formulation of the ADO-PUA resins used in the study\*.

R-Value ( $\frac{H12MDI}{ADO + PTMEG + PDMS}$ )	Sample	H <sub>12</sub> MDI (NCO*2)	ADO (OH*2)	PTMEG (OH*2)	PDMS (OH*2)	HEA (Acrylate-Capping)
3.0	PUA <sub>3.0</sub> -ADO <sub>1.0</sub>	9.0	1.0	1.0	1.0	12.0
2.5	PUA <sub>2.5</sub> -ADO <sub>1.0</sub>	7.5				9.0
2.2	PUA <sub>2.2</sub> -ADO <sub>1.0</sub>	6.6				7.2
2.0	PUA <sub>2.0</sub> -ADO <sub>1.0</sub>	6.0				6.0
1.8	PUA <sub>1.8</sub> -ADO <sub>1.0</sub>	5.4				4.8
1.6	PUA <sub>1.6</sub> -ADO <sub>1.0</sub>	4.8				3.6
1.4	PUA <sub>1.4</sub> -ADO <sub>1.0</sub>	4.2				2.4
1.2	PUA <sub>1.2</sub> -ADO <sub>1.0</sub>	3.6				1.2
2.0	PUA <sub>2.0</sub> -ADO <sub>0.0</sub>	4.0	0	1.0	1.0	4.0
	PUA <sub>2.0</sub> -ADO <sub>0.5</sub>	5.0	0.5			5.0
	PUA <sub>2.0</sub> -ADO <sub>1.0</sub>	6.0	1.0			6.0
	PUA <sub>2.0</sub> -ADO <sub>2.0</sub>	8.0	2.0			8.0
	PUA <sub>2.0</sub> -ADO <sub>4.0</sub>	12.0	4.0			12.0

\* The samples were prepared by 3D-printing in the study as shown in Fig. S4.

stretching at  $3280\text{ cm}^{-1}$  [36] can be observed (Fig. S1). Additionally, from <sup>1</sup>H NMR (Fig. S2), the PUA structure of the three signals at 6.4 ppm, 6.2 ppm, and 5.9 ppm are attributed to the  $-\text{CH}=\text{CH}_2$  from the 2-hydroxyethyl acrylate. Compared to the PUA resin without addition of ADO and PTMS, the new characteristic signals located at 2.2–2.6 ppm, 1.2–1.4 ppm, and 0.1–0.2 ppm are the cause of protons of ADO and PDMS, respectively [31,37].

The molecular weight distributions of resins with different R values at each step of the synthesis reaction are monitored by GPC (Fig. S3).

Both the average molecular weight  $M_n$  and  $M_w$  of the prepolymers gradually increase with the addition of reactants. The polydispersity (PDI) of the prepolymers is also well controlled in each synthesis step, as shown in Table S1. Thus, from the above results of the FT-IR NMR spectra, and GPC, UV-curable PUA resin has been well prepared through the synthesis reaction. Subsequently, this range of synthesized resins was used to fabricate thin substrates via LCD 3D printing to investigate their fundamental properties.

### 3.2. R-value adjustment for ADO-PUA resin

The mechanical property of the ADO-PUA resins can be adjusted by the R-value, which is the ratio between isocyanate and hydroxyl groups. This is because elongation and tensile strength depend on the influence of hard and soft segments or, more precisely, on the overall morphology of the copolymer. The average molecular chain length ( $M_c$ ) between neighboring sites in a crosslinked sample is shortened due to the shorter PUA chains at high R values [32]. However, the higher the isocyanate content of the PUA resin, the harder the fabricated sample will be, and the brittleness may even cause cracks in the printing process. Therefore, the proper R-value is an important factor in the mechanical properties of PUA resin products. First, the R-value of the ADO-PUA resin formulation was adjusted from 1.2 to 3.0 for a fixed ADO mole fraction. As shown in Fig. 2(a), the tensile strength of the PUA substrate decreased with the decrease of the R-value of the PUA resin, while the elongation at break (%) increased significantly due to the fact that the high R-value PUA chains contained a large number of isocyanates with a rigid hexagonal structure, which reduced the mobility of the copolymer chains. Among them, resins with R-values of 2.2 and 2.0 exhibit superior elongation at break (exceeding 100%), ultimate tensile strengths above 10 MPa, and toughness around 10 MPa, making them more suitable for printing flexible 3D objects with good flexibility and mechanical strength.

The Dk and Df of the PUA resins are also measured to study their dielectric properties. Both Dk and Df are closely related to the polarizability, but only Dk can be reduced by increasing the free volume in the polymer matrix. As shown in Fig. 2(b), there is little difference in the dielectric properties of the resins with different R values. Yet, the ADO-PUA resins have lower Dk and Df values compared to the commercial MMA resin (purchased from 3D Pro. Works Co., Ltd., Taiwan) and PCB material (High  $T_g$  FR-4). The introduction of adamantane into the polymer main chain can effectively reduce the Dk, especially the formulations with R-values of 2.0 and 1.8 have slightly better Dk than the other R-values. The polarity of PUA varies with its component segments, but its R value only reflects the amount of urethane (carbamate) links. Therefore, the R value can only partially represent the polarity in the resin formulation. Consequently, Df does not exhibit a monotonous dependence with R-value but shows a minimum at PUA2.0. After considering the above inherent mechanical properties and the basic dielectric properties, further investigation was conducted to optimize the dielectric properties of the ADO-incorporated photocurable resin based on an R-value of 2.0, by investigating different molar ratios of ADO. Table S2 lists the results of the mechanical and dielectric properties of 3D-printed substrates made with ADO-PUA resins of different R-values.

### 3.3. Optimization with ADO content

Optimizing the ADO content in PUA resins not only improves the mechanical properties, but also increases the  $V_f$  and thus reduces the dielectric constant [38–40]. As can be seen from Fig. 3(a), with the increasing ADO content, the tensile strength of the PUA substrate increased and the elongation at break decreased, which is consistent with the aforementioned literature results [30,31]. Additionally, the modulus of toughness defines the energy required to break the material and it can be calculated from the area under the stress-strain curve in Fig. S5. The results indicated that the moderate introduction of ADO contributed to improving the tensile strength of the PUA-printed substrates and maintained their flexibility. As can be seen, introducing an appropriate amount of ADO in the resin backbone can improve the toughness of the 3D-printed substrate. However, A high concentration of ADO causes an increase in the steric effect, which makes it difficult for each printed layer of the sample to be tightly bonded during the 3D printing process, resulting in incomplete and poorly structured 3D printed objects. Thus, the comprehensive mechanical properties of the ADO<sub>1,0</sub> and ADO<sub>2,0</sub> formula are superior to other series of PUA resins, and it seems to be more suitable for flexible substrates.

As the molar ratio of ADO in PUA resin increases, Dk value gradually decreases due to the increase in the  $V_f$  of the structure, as shown in Fig. 3(b). However, the introduction of adamantane did not significantly improve the loss tangent (Df) reduction. Although the symmetry of the overall structure of the PUA polymer was improved by selecting symmetrical raw materials in the synthesis stage, the reduction of the Df value was still limited (The optimal Df value is around 0.02, which is similar to the value of a High  $T_g$  FR-4). The main reason is that the overall polarity of the structure is affected by the amide (NH) and carbonyl (C=O) of the urethane and acrylic groups, and it was not easy to offset. In addition, the inversion in the Df of PUA<sub>2,0</sub>-ADO<sub>4,0</sub> is slightly unusual. We speculate that the addition of excessive ADO may lead to the accumulation of molecular segments, resulting in a minor abnormality in the Df performance of PUA<sub>2,0</sub>-ADO<sub>4,0</sub>. So far, it is also worth noting that the Dk and Df values of the UV-curable resin, PUA<sub>2,0</sub>-ADO<sub>1,0</sub>, and PUA<sub>2,0</sub>-ADO<sub>2,0</sub>, were significantly better than those of the commercial resin (MMA resin, Dk = 3.2612 and Df = 0.035) and PCB material (High  $T_g$  FR-4, Dk = 4 and Df = 0.02) [41]. Table S3 lists the mechanical and dielectric property results for PUA<sub>2,0</sub> resins with different ADO contents. The above results indicate that the introduction of adamantane into the polymer matrix can effectively improve the dielectric properties, especially the reduction of the Dk value is the most significant. In a comparative assessment, the incorporation of an optimal quantity of ADO has proven to be instrumental in achieving superior flexibility and dielectric properties. Among the formulations examined, both PUA<sub>2,0</sub>-ADO<sub>1,0</sub> and PUA<sub>2,0</sub>-ADO<sub>2,0</sub> resins excelled in flexibility and

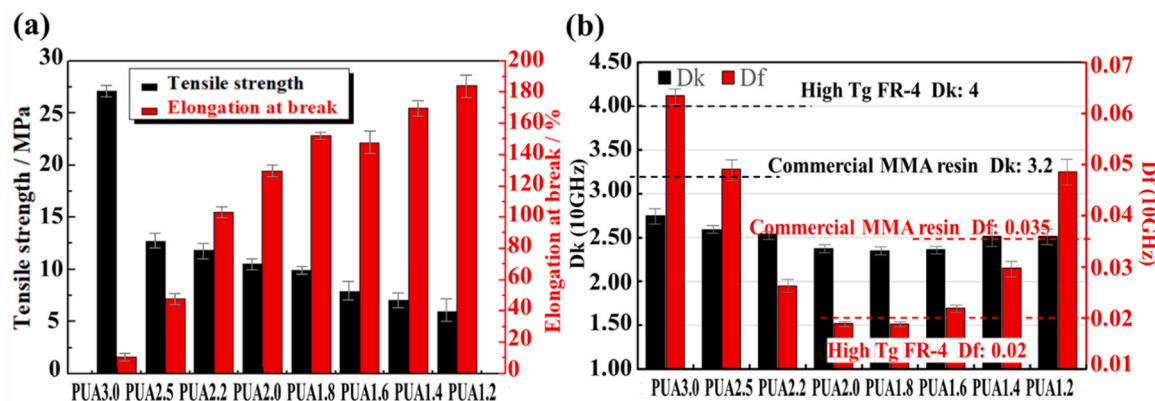
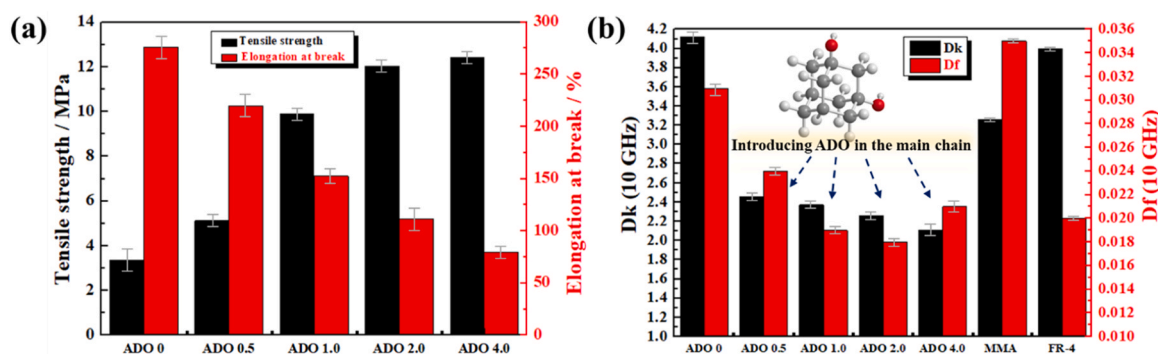


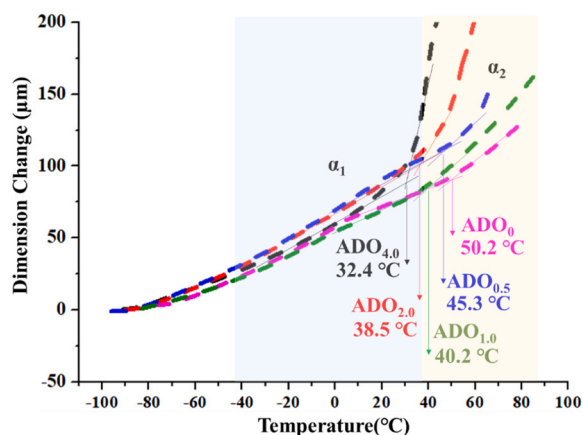
Fig. 2. (a) Mechanical properties of 3D-printed substrates made with ADO-PUA resins of different R-values. (b) Dk and Df values of 3D-printed substrates made with ADO-PUA resins of different R-values.



**Fig. 3.** (a) The mechanical properties of 3D-printed substrates with different ADO content in PUA<sub>2.0</sub> resin. (b) Dk and Df values of 3D-printed substrates with different ADO content in PUA<sub>2.0</sub> resins.

dielectric properties. Thermal stability is discussed further in the next section. This discussion is again based on the 2.0 R-value of the resin formulation, aimed at identifying the final ideal composition of the UV-curable resin for this study.

To further illustrate the effect of the introduction of adamantane on the  $V_f$  of the polymer chain, we measured the changes in thermal expansion of each sample using TMA. These dimension changes are correlated with variations in the free volume of the polymer. The coefficients of linear thermal expansion ( $\alpha_{1,v}$ , and  $\alpha_{2,v}$ ) are evaluated from the linear segments of the measured plots. Moreover, the phase transition temperature  $T_g$  can also be determined by identifying the intersection of the extrapolated linear parts of the plots. In Fig. 4, the thermal expansion behavior of all the ADO-contained samples is illustrated over a broad temperature range, ranging from  $-90$  to  $90$  °C. Assuming isotropic behavior, the relation  $\alpha_{i,v} = 3\alpha_i$  can be used to convert the coefficients into coefficients of volume expansion ( $\alpha_{1,v}$ ,  $\alpha_{2,v}$ ), as shown in Table 2. The results show the increases in  $\alpha_{1,v}$  value (thermal expansion below  $T_g$ ) with increasing ADO content, indicating that the mobility of chain constituents is less restricted in the rigid state and the introduction of adamantane increases the  $V_f$ . Similarly, above  $T_g$ , samples with higher ADO content show higher  $\alpha_{2,v}$  values in the thermal expansion behavior. The highest expansivity observed in resins with higher ADO content can also be used to check the free volume variation by calculating the differences in the thermal expansions,  $\alpha_{1,v}-\alpha_{2,v}$ . The results further confirm that with the increase of ADO, higher  $V_f$ , and less cross-linked structure can be obtained. In addition, cross-linked structures can also be verified by comparison of gel fractions. Fig. S5 shows the gel fraction of 3D printing substrates with different ADO contents. With the increased addition of ADO, the molecular structures undergo gradual alteration (less cross-linked) and reflect in even lower gel



**Fig. 4.** TMA plots of 3D-printed substrates with different ADO content in PUA<sub>2.0</sub> resin.

**Table 2**

Coefficients of volume expansion and phase transition temperature  $T_g$  of 3D-printed substrates with different ADO contents.

Sample	$T_g$ [°C]	$\alpha_{1,v}$ [ $\mu\text{m}/\text{m}\cdot\text{°C}$ ]	$\alpha_{2,v}$ [ $\mu\text{m}/\text{m}\cdot\text{°C}$ ]	$\alpha_{1,v}-\alpha_{2,v}$ [ $\mu\text{m}/\text{m}\cdot\text{°C}$ ]
PUA <sub>2.0</sub> -ADO <sub>0</sub>	50.2	288.8	296.2	7.4
PUA <sub>2.0</sub> -ADO <sub>0.5</sub>	45.3	299.5	326.2	26.7
PUA <sub>2.0</sub> -ADO <sub>1.0</sub>	40.2	316.5	351.5	35.0
PUA <sub>2.0</sub> -ADO <sub>2.0</sub>	38.5	339.1	401.7	62.6
PUA <sub>2.0</sub> -ADO <sub>4.0</sub>	32.4	342.2	528.9	186.7

fractions. This is consistent with the research report mentioned in the introduction [28–31], indicating that the bulky three-dimensional structure of the adamantane group can lower the cross-link density of the polymer, increase the free volume, improve the mechanical, and dielectric properties of polymers.

### 3.4. Thermal stability of PUA<sub>2.0</sub>-ADO resins

TGA analysis of 3D-printed substrates prepared from a series of PUA<sub>2.0</sub> resins with different ADO content is shown in Fig. 5(a). The decomposition temperatures ( $T_d$ ) of these samples at  $T_d5\%$ ,  $T_d10\%$ , and  $T_d50$ , and the main weight loss regions with peak maximum in the DTG curves are listed in Table 3. Prior to testing, all samples were vacuum dried at  $90$  °C for 20 minutes to remove moisture. As shown in Fig. 5(b), the DTG curve has two main weight loss peaks, and the maximum peaks are around  $320$  °C and  $430$  °C, indicating that the decomposition stage of the 3D-printed samples can be divided into two stages. In general, the decomposition of small amounts of organic molecules and the volatilization of solvents caused weight loss before  $200$  °C. The first thermal decomposition stage of the samples began around  $300$  °C to  $330$  °C, in which the urethane functional groups (hard segments) were eliminated, and the second decomposition peak (around  $430$  °C) is caused by the soft chain breakage and the degradation of carbonaceous residues, which is attributed to the breakage of C-C bonds. Upon comparing with literature reports (listed in Table 3), the thermal stability of the investigated samples is significantly higher than that of the conventional PUA resins [42–46]. For all 3D-printed samples containing ADO, the first major weight loss temperature ( $DTG_1$ ) exceeded  $320$  °C, and the second weight loss ( $DTG_2$ ) of PUA<sub>2.0</sub>-ADO<sub>4.0</sub> resin even occurred above  $430$  °C. This result can be attributed to the incorporation of ADO into the polymer backbone and the cross-linking effect of TMPTA, which improved the thermal properties of the material. In particular, the introduction of rigid segments into the polymer backbone can increase the thermal stability and glass transition temperature ( $T_g$ ) of the corresponding

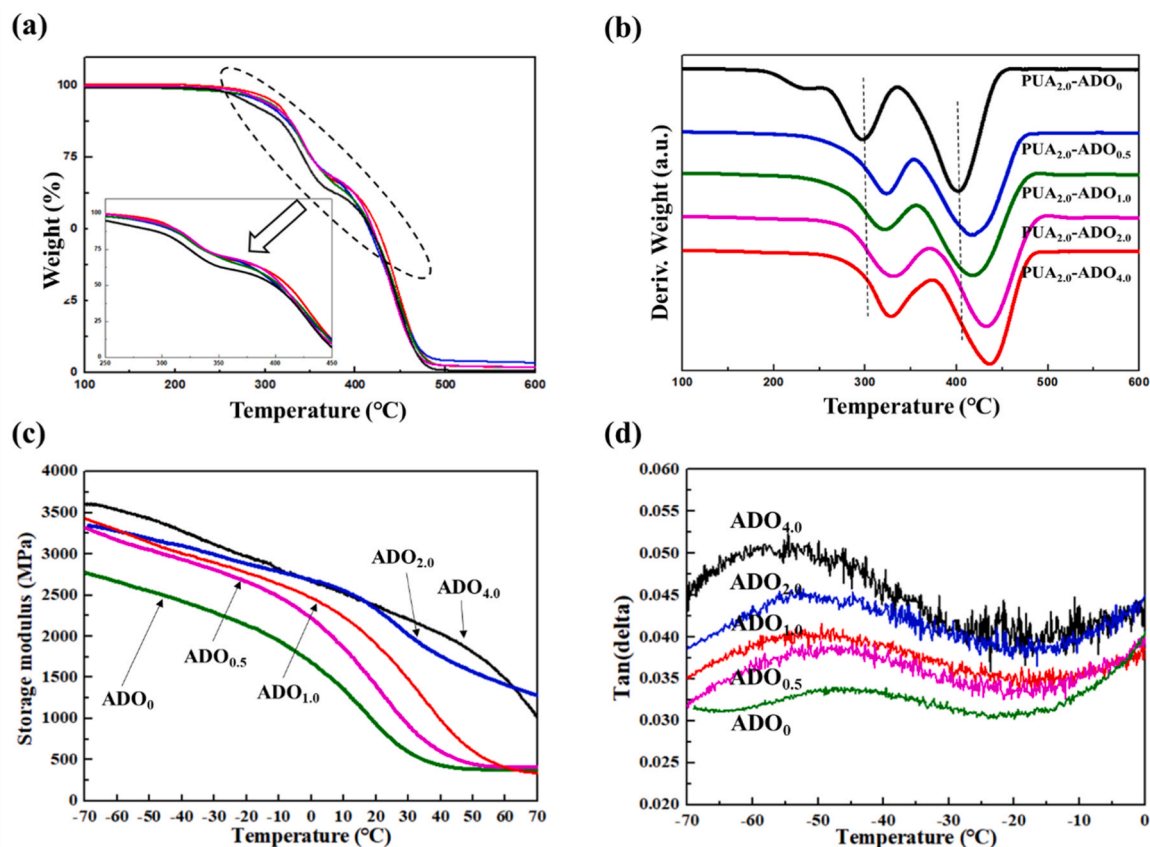


Fig. 5. (a) The TGA analysis of 3D-printed substrates with different ADO content in PUA<sub>2.0</sub> resin. (b) The DTG curves of 3D-printed substrates with different ADO content in PUA<sub>2.0</sub> resin. (c) DMA storage modulus E' and (d) tan  $\delta$  of 3D-printed substrates.

**Table 3**  
Comparison of thermal stability of PUA-related polymers.

Sample	Decomposition Temperature (°C)			Peak of Derive. Weight (°C)		Reference
	T <sub>d</sub> 5%	T <sub>d</sub> 10%	T <sub>d</sub> 50%	DTG <sub>1</sub>	DTG <sub>2</sub>	
PUA <sub>2.0</sub> -ADO <sub>0</sub>	258	276	397	301	404	
PUA <sub>2.0</sub> -ADO <sub>0.5</sub>	290	301	400	321	417	
PUA <sub>2.0</sub> -ADO <sub>1.0</sub>	292	302	403	322	418	
PUA <sub>2.0</sub> -ADO <sub>2.0</sub>	293	307	405	324	428	
PUA <sub>2.0</sub> -ADO <sub>4.0</sub>	300	309	412	328	436	
Waterborne PUA (Optimal Value)	118	152	370	N/A	N/A	[43]
Waterborne PUASi10 (Optimal Value)	N/A	301	398	386	417	[44]
PUA S4 (Optimal Value)	231.5	N/A	363.3	333	417	[45]
PUA-25 wt% Li	N/A	N/A	N/A	305	448	[46]
PDMS-WPUA20%	273	N/A	N/A	330	418	[47]

polymer [47–49]. The improved thermal stability of ADO-incorporated photocurable resin was attributed to the unique "diamond-like" cage structure of adamantane, which can inhibit the degradation reactions [48]. Overall, the thermal stability of photocurable PUA resins in the study increased with the increase of ADO content, which was consistent with the above literature results. It can be seen that PUA<sub>2.0</sub>-ADO<sub>4.0</sub> resin exhibits the most stable thermal properties among a series of PUA<sub>2.0</sub> resin series. Therefore, based on the evaluation of the above results, including mechanical properties, Dk and Df values, and thermal stability, the PUA<sub>2.0</sub>-ADO<sub>2.0</sub> resin will be employed as the 3D printing material in the subsequent sections.

Additionally, the dynamic mechanical properties of PUA<sub>2.0</sub> resins

were investigated with DMA, which revealed a change in the glass transition temperature (T<sub>g</sub>), defined as peak of tan ( $\delta$ ), of the soft segments. Fig. 5(c) and (d) show the storage modulus and tan ( $\delta$ ) for PUA<sub>2.0</sub> resins. As shown in Fig. 5(c), the storage modulus enhanced upon increasing ADO content in the resin, indicating a greater stiffness of the printed substrate. Compared with PUA<sub>2.0</sub>-ADO<sub>0</sub> resin (without introducing ADO in the main chain), substrates with high ADO content were more resistant to the decrease in storage modulus as the temperature increased. The substrate with high ADO content was conducive to maintaining a certain stiffness at room temperature and was more suitable for the subsequent electroless plating process. The soft segments of PUA resins (polyether chains) account for the elastic behavior. In general, the T<sub>g</sub> of soft segments in PUA resin is around  $-50$  °C [50]. As shown in Fig. 5(d), high ADO-containing substrate exhibited lower T<sub>g</sub> (below  $-50$  °C). Due to the large steric hindrance of ADO, the formation of hydrogen bonds between polyether segments in the main chain of PUA resin is hindered, which is conducive to the free movement of polymer chain [31]. In this case, the maximum of tan ( $\delta$ ) shifted toward lower temperatures.

### 3.5. Reducing the Df value of the PUA<sub>2.0</sub>-ADO<sub>2.0</sub> resin

Although the Dk (dielectric constant) values of the photocurable resins have been successfully reduced by the introduction of 1,3-adamantanediol, the reduction of Df (loss tangent) values in the study is still limited due to the inherent properties of the polyurethane-based materials. Using BN as a filler can alleviate this problem a little. The percentage of BN powder added to the resin varies from 0.05 wt% to 5 wt%, as the use of small amounts of BN powder allows better control of its dispersion in the resin. Higher concentrations of BN in the resin have not been studied because high concentrations and aggregation of BN

powders may result in a less-than-optimal photocuring process. The dielectric properties of the photocurable resin (PUA<sub>2.0</sub>-ADO<sub>2.0</sub>) blended with BN powder are shown in Fig. 6(a). It can be seen that the Df value decreased with the increase of the BN powder addition ratio. However, since the inherent Dk value of BN is higher than that of the PUA<sub>2.0</sub>-ADO<sub>2.0</sub> resin, its addition also affects the Dk value. The result shows that a BN content of 0.5 wt% to 1 wt% is the optimal addition proportion to obtain ideal dielectric composites. Compare with the Df of PUA<sub>2.0</sub>-ADO<sub>2.0</sub> resin, the Df of PUA<sub>2.0</sub>-ADO<sub>2.0</sub>-BN<sub>0.5 wt%</sub> resin was reduced to 0.005, while its Dk still maintained its low dielectric properties (Dk~2.65). Table 4 shows the measured Dk and Df of PUA<sub>2.0</sub>-ADO<sub>2.0</sub> resin with BN powder added.

In order to determine the feasibility of using low Dk photocurable resins in 5 G devices, we performed a comprehensive evaluation by measuring the S-parameters, specifically the insertion loss (S<sub>21</sub>) and return loss (S<sub>11</sub>) of the metallized substrate antenna. These measurements were performed using a precision vector network analyzer. The use of S-parameters proved to be helpful in gaining a comprehensive understanding of the behavior of signals as they pass through interconnecting lines similar to transmission lines.

A comparison of the signal integrity of 3D printed microstrip plates made from commercial MMA resin, high Tg FR-4, and the low Dk photocurable resin formula developed in this study is shown in Fig. 6(b). The smaller the absolute value of S<sub>21</sub>, the lower the insertion loss on the circuit board. Obviously, the test vehicles printed with the low Dk photocurable resin formulations show lower S<sub>21</sub> attenuation below 10 GHz than commercial MMA resins and high Tg FR-4. Fig. 6(c) shows that the insertion loss of PUA<sub>2.0</sub>-ADO<sub>2.0</sub> resin formulation with BN is less than 2.5 dB up to 6 GHz. Generally, WIFI and Bluetooth antennas for

consumer electronics typically operate at 2.4 and 6 GHz, so the excellent S<sub>21</sub> performance of the low Dk photocurable resin developed in this study is a good demonstration of its potential for LCP 3D fabrication of these components. As shown in Fig. 6(d), the return loss (S<sub>11</sub>) of the low Dk photocurable resin is mostly higher than 10 dB below 10 GHz, demonstrating high signal reflection. The measured values of the metallized substrate antenna parameters proved to be within the acceptable range for 5 G devices.

### 3.6. Adhesion of copper plating

Based on the above experimental results, we found that PUA<sub>2.0</sub>-ADO<sub>2.0</sub>-BN<sub>1 wt%</sub> has the potential to be used as a suitable material for 3D printing photocurable resin for electronic devices in the 5 G era. Besides excellent dielectric, thermal and mechanical properties, products printed with this resin can also be used for metallization. Surface pretreatment is an important process for substrate metallization to improve adhesion. Surface pretreatment of the substrate is divided into a dry process and a wet process. Plasma treatment of polymers is an environmentally-friendly method with low energy consumption to activate the polymer surface and does not affect the intrinsic properties of the original material. As shown in Fig. 7(a), compared with the non-plasma-treated substrate, no copper deposits were peeled off from the plasma-treated substrate even after the removal by the test tape (3 M 600). In contrast, the substrate that has not been plasma treated shows poor adhesion between copper deposits and the substrate surface. This behavior indicates that the adhesion of metallized UV-curable PUA resins can be significantly improved by oxygen plasma treatment. Further, adhesion testing was performed to understand the adhesion between the

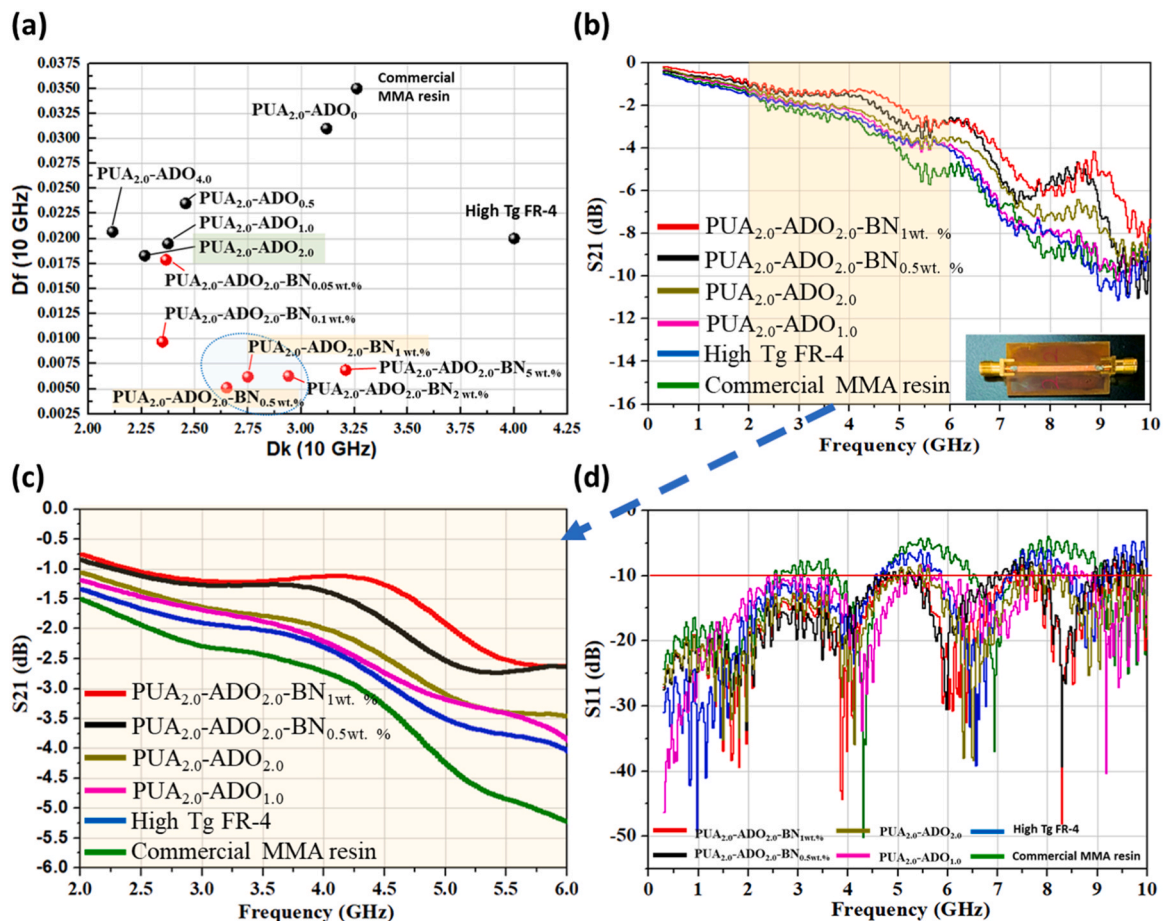






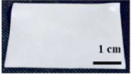
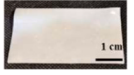
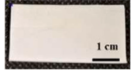
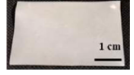
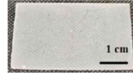

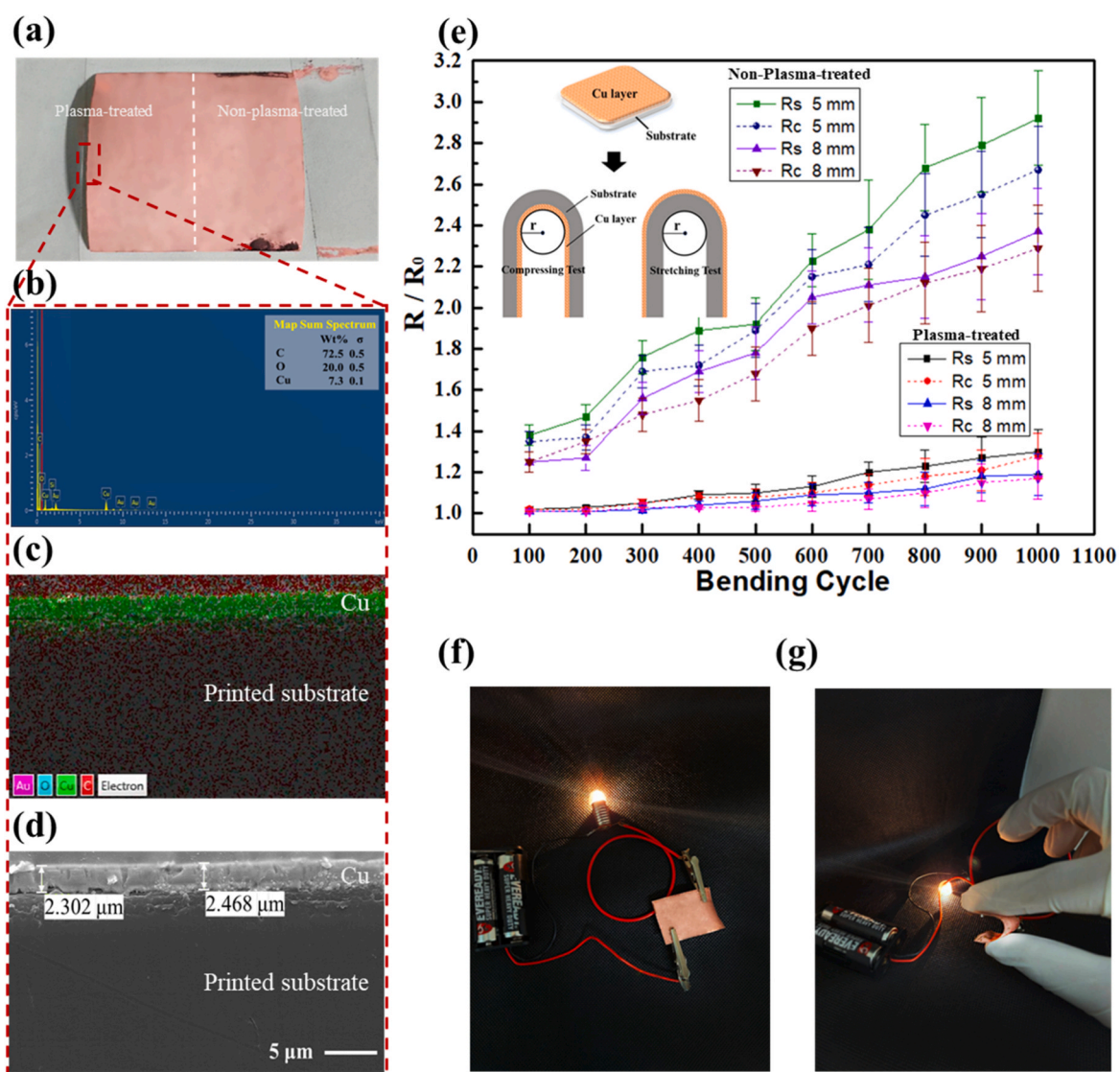


Fig. 6. (a) Dielectric properties of PUA<sub>2.0</sub>-ADO<sub>2.0</sub> resin blended with BN powder. (b)-(c) Measured S<sub>21</sub> and (d) S<sub>11</sub> of micro-strip line tests. The micro-strip line test vehicle is printed on a plate made by the cured low Dk resin.



**Table 4**  
Dielectric properties of PUA<sub>2.0</sub>-ADO<sub>2.0</sub> resin with BN powder addition.

	PUA <sub>2.0</sub> -ADO <sub>2.0</sub> -BN <sub>5</sub> wt%	PUA <sub>2.0</sub> -ADO <sub>2.0</sub> -BN <sub>2</sub> wt%	PUA <sub>2.0</sub> -ADO <sub>2.0</sub> -BN <sub>1</sub> wt%	PUA <sub>2.0</sub> -ADO <sub>2.0</sub> -BN <sub>0.5</sub> wt%	PUA <sub>2.0</sub> -ADO <sub>2.0</sub> -BN <sub>0.1</sub> wt%	PUA <sub>2.0</sub> -ADO <sub>2.0</sub> -BN <sub>0.05</sub> wt%
BN added in resin						
Printed substrates						
Dk	3.21	2.94	2.75	2.65	2.35	2.37
Df	0.0069	0.0063	0.0062	0.0051	0.0097	0.0179



**Fig. 7.** (a) After metallization, the adhesion test results for the plasma-treated substrate and the non-plasma-treated substrate. Results of a cross-sectional analysis of metalized substrate by (b) EDS elemental spectrum. (c) EDS mapping. (d) SEM image. (e) The relative resistance increase (R/R<sub>0</sub>) versus the number of bending cycles tested using two different bending radii of curvature (5 mm and 8 mm). (f) The printed substrate connected to a power supply. (g) The metalized samples remained conductive during bending.

metal and substrate. When ASTM D3359 is a standard test method for measuring adhesion by tape test. In the case of oxygen-plasma treatment, copper depositions successfully remained on the surface of the 3D printed substrate after 64 tape-removing cycles, indicating the level of 4B to 5B adhesion, as shown in Fig. S6. After the electroless plating process, the thickness of the Cu layer was obtained by averaging photos of 5 cross-sectional SEM images. As shown in Fig. 7(b)-(d), the cross-sectional SEM image showed the average thickness of the Cu layer (about 2.385  $\mu\text{m}$ ), and the EDS analysis demonstrated Cu contents. XRF is well-suitable for the non-destructive analysis of metals in a thin film. The analysis of XRF in Fig. S7 indicates that the average thickness of the Cu layer was about 2.562  $\mu\text{m}$  when the electroless plating time was 20 min, and it was uniform and tightly bonded to the substrate. The excellent adhesion confirms the viability of our fabricated PUA resins in bendable circuit boards and other flexible electronics.

The bending fatigue durability of metallized substrates is pivotal for the practical application of flexible electronics. Cyclical bending tests of  $-180^\circ$  cyclic compressing or  $+180^\circ$  cyclic stretching bending tests were performed at a cycle frequency of 100 cycles/min using a customized apparatus to assess the fatigue resistance. Fig. 7(e) shows the relative resistance increase ( $R/R_0$ ) versus the number of bending cycles tested using two different bending radii of curvature (5 mm and 8 mm), where  $R_0$  and  $R$  represent the electrical resistance before and after bending, respectively. The 5 mm radius is the basic requirement to ensure the conductive robustness of metallized substrates in practical applications. The bending test results for 5 mm and 8 mm radii demonstrated that the conductivity was quite robust against mechanical bending. Especially for the standard test with a 5 mm radius, the electrical resistance only increased by 28% after 1000 stretching cycles. The metallized substrate was connected to a bulb via two wires and a 3.0 V direct-current (DC) voltage supply as shown in Fig. 7(f) and Fig. 7(g).

### 3.7. Feasibility of printing 3D objects

To confirm the feasibility of LCD 3D printing for electronic devices, the formulated resin is printed into 3D objects and metallized. As a proof of concept, a 3D hollow object and its metallization are shown in Fig. 8 (a) and Fig. 8(b). 3D printed object showed excellent printing fidelity and precision compared to their original CAD models and is electrically conductive (Fig. 8(c)). 3D structures printed with this PUA<sub>2.0</sub>-ADO<sub>2.0</sub>-BN<sub>1</sub> wt% resin is feasible and very reliable after metallization, even for small patterns of 3D structures. The 3D wearable band and frame-like architectures of the photocurable resin were LCD-printed, as shown in Fig. 9(a). It shows the excellent resolution quality of the 3D printed wearable band. As shown in Fig. 9(b), the printed 3D wearable frame was able to be attached to a smartwatch and resized to fit the wrist. On the whole, it is feasible to print 3D structured objects with this resin

formulation. In conclusion, the formulated low-K PUA resin can be used to fabricate metallized flexible substrates by 3D printing technique and electroless plating process, opening up numerous opportunities for soft electronics in 5 G applications.

## 4. Conclusion

A series of PUA resins with different R-values and ADO contents are synthesized, and their subsequent dielectric properties, mechanical properties, thermal stability, metallization adhesion, and electrical conductivity of 3D printed substrates are optimized. The results showed that resins with R-values of 2.0 displayed lower Dk values, Df values, and better mechanical properties compared to resins with other R-values. Additionally, the increment of ADO content contributed to the decrease of the Dk. Most notably, the introduction of 1,3-adamantane-diol into the polymer backbone of 3D printed materials can effectively lower the electrical constant. Among them, the PUA<sub>2.0</sub>-ADO<sub>2.0</sub> not only exhibited the lowest dielectric constant (Dk: 2.26 and Df: 0.018 @10 GHz), but also showed high thermal stability (Td<sub>5%</sub>: 293  $^\circ\text{C}$ , Td<sub>10%</sub>: 307  $^\circ\text{C}$ , and Td<sub>50%</sub>: 405  $^\circ\text{C}$ ) and great mechanical properties (tensile strength 12.02 MPa and elongation break at 111.35%), which was better than that reported for UV-cured polyurethane elastomers and the 3D commercial resin. With little addition of BN powder (1 wt%), the Df of PUA resin can also be effectively reduced (Df: 0.006), and the measured values of its metallized substrate antenna parameters are proven to be within the acceptable range for 5 G devices. The metallized substrates exhibited excellent adhesion, passing the adhesion test to Class 5B. These characteristics are sufficient for the practical applications in 3D printing technology, especially since the low dielectric constant has the opportunity to replace traditional rigid FR-4 substrates in the application of 5 G flexible boards and films. In summary, a novel synthetic method is successfully developed to prepare low-dielectric constant resin for LCD 3D printing. This research opens new ground for the development of UV-curable formulations in flexible 3D architectures.

### CRediT authorship contribution statement

**Yu-Ho Chen:** Validation, Methodology. **I-Tsung Liu:** Writing – review & editing, Visualization. **Shih-Huang Tung:** Writing – review & editing, Supervision. **Ramachandran Balaji:** Writing – review & editing, Software. **Jhu-Lin You:** Writing – original draft, Methodology, Investigation, Formal analysis, Data curation, Conceptualization. **Ying-Chih Liao:** Writing – review & editing, Supervision, Funding acquisition, Conceptualization.

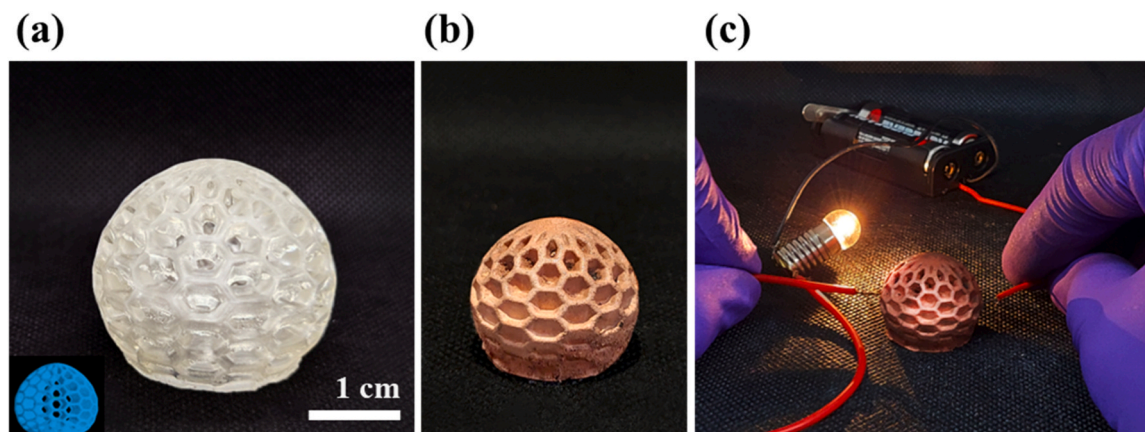


Fig. 8. (a) a 3D hollow object. (d) The printed object after metallization. (c) The 3Dprinted object exhibits high conductivity.

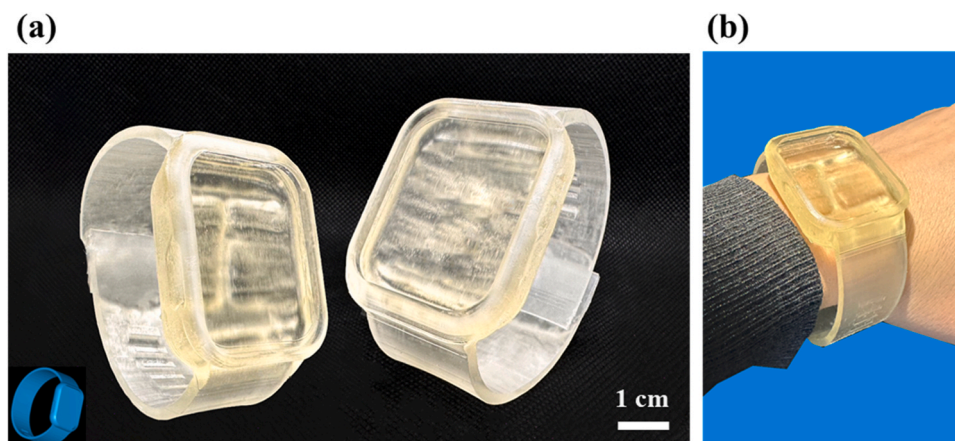


Fig. 9. (a)-(b) Photographs of 3D wearable PUA band applied to a practical smartwatch.

### Declaration of Competing Interest

The authors declare no conflicts of interest.

### Data availability

Data will be made available on request.

### Acknowledgements

This study is supported by the National Science and Technology Council in Taiwan (NSTC 112-2221-E-002 -026 -MY3 and NSTC112-2622-E-002-035), and National Taiwan University (NTUCC-111L4000-1).

### Appendix A. Supporting information

Supplementary data associated with this article can be found in the online version at [doi:10.1016/j.addma.2024.104047](https://doi.org/10.1016/j.addma.2024.104047).

### References

- [1] S.-C. Tsai, L.-H. Chen, C.-P. Chu, W.-C. Chao, Y.-C. Liao, Photo curable resin for 3D printed conductive structures, *Addit. Manuf.* 51 (2022) 102590.
- [2] J. Li, C. Boyer, X. Zhang, 3D printing based on photopolymerization and photocatalysts: review and prospect, *Macromol. Mater. Eng.* 307 (8) (2022) 2200010.
- [3] D. Bozoglu, H. Deligoz, K. Ulutas, S. Yakut, D. Deger, Structural and dielectrical characterization of low-k polyurethane composite films with silica aerogel, *J. Phys. Chem. Solids* 130 (2019) 46–57.
- [4] H. Zhao, S.-Q. Zhao, Q. Li, M.R. Khan, Y. Liu, P. Lu, C.-X. Huang, L.-J. Huang, T. Jiang, Fabrication and properties of waterborne thermoplastic polyurethane nanocomposite enhanced by the POSS with low dielectric constants, *Polymer* 209 (2020) 122992.
- [5] X. Ji, D. Chen, J. Shen, S. Guo, Flexible and flame-retarding thermoplastic polyurethane-based electromagnetic interference shielding composites, *Chem. Eng. J.* 370 (2019) 1341–1349.
- [6] S. Liu, R. Duan, S. He, H. Liu, M. Huang, X. Liu, W. Liu, C. Zhu, Research progress on dielectric properties of PU and its application on capacitive sensors and OTFTs, *React. Funct. Polym.* (2022) 105420.
- [7] X. Wu, J. Zhang, H. Li, H. Gao, M. Wu, Z. Wang, Z. Wang, Dual-hard phase structures make mechanically tough and autonomous self-healable polyurethane elastomers, *Chem. Eng. J.* 454 (2023) 140268.
- [8] Z. Hu, X. Liu, T. Ren, H.A. Saeed, Q. Wang, X. Cui, K. Huai, S. Huang, Y. Xia, K. Fu, Research progress of low dielectric constant polymer materials, *J. Polym. Eng.* 42 (8) (2022) 677–687.
- [9] C. Mendes-Felipe, T. Rodrigues-Marinho, J.L. Vilas, S. Lanceros-Mendez, UV curable nanocomposites with tailored dielectric response, *Polymer* 196 (2020) 122498.
- [10] L. Xiong, D. Li, Y. Yang, X. Ye, Y. Huang, E. Xu, C. Xia, M. Yang, Z. Liu, X. Cui, Tailoring crosslinking networks to fabricate photocurable polyurethane acrylate (PUA) dielectric elastomer with balanced electromechanical performance, *React. Funct. Polym.* 183 (2023) 105498.
- [11] D. Kwon, T.-I. Lee, J. Shim, S. Ryu, M.S. Kim, S. Kim, T.-S. Kim, I. Park, Highly sensitive, flexible, and wearable pressure sensor based on a giant piezocapacitive effect of three-dimensional microporous elastomeric dielectric layer, *ACS Appl. Mater. Interfaces* 8 (26) (2016) 16922–16931.
- [12] S. Chen, B. Zhuo, X. Guo, Large area one-step facile processing of microstructured elastomeric dielectric film for high sensitivity and durable sensing over wide pressure range, *ACS Appl. Mater. Interfaces* 8 (31) (2016) 20364–20370.
- [13] W. Yang, N.W. Li, S. Zhao, Z. Yuan, J. Wang, X. Du, B. Wang, R. Cao, X. Li, W. Xu, A breathable and screen-printed pressure sensor based on nanofiber membranes for electronic skins, *Adv. Mater. Technol.* 3 (2) (2018) 1700241.
- [14] X. Yin, Y. Feng, Q. Zhao, Y. Li, S. Li, H. Dong, W. Hu, W. Feng, Highly transparent, strong, and flexible fluorographene/fluorinated polyimide nanocomposite films with low dielectric constant, *J. Mater. Chem. C* 6 (24) (2018) 6378–6384.
- [15] S. Nayak, B. Sahoo, T.K. Chaki, D. Khastgir, Development of polyurethane–titania nanocomposites as dielectric and piezoelectric material, *RSC Adv.* 3 (8) (2013) 2620–2631.
- [16] N. Hong, Y. Zhang, Q. Sun, W. Fan, M. Li, M. Xie, W. Fu, The evolution of organosilicon precursors for low-k interlayer dielectric fabrication driven by integration challenges, *Materials* 14 (17) (2021) 4827.
- [17] P. Bhashpa, K. Bijudas, T. Francis, Enhanced dielectric and thermal properties of thermoplastic polyurethane/multi-walled carbon nanotube composites, *Mater. Today Proc.* 51 (2022) 2254–2259.
- [18] W. Li, X. Jin, Y. Zheng, X. Chang, W. Wang, T. Lin, F. Zheng, O. Onyilgha, Z. Zhu, A porous and air gap elastomeric dielectric layer for wearable capacitive pressure sensor with high sensitivity and a wide detection range, *J. Mater. Chem. C* 8 (33) (2020) 11468–11476.
- [19] V. Jousseume, J. El Sabahy, C. Yeromonahos, G. Castellan, A. Bouamrani, F. Ricoul, SiOCH thin films deposited by chemical vapor deposition: from low- $\kappa$  to chemical and biochemical sensors, *Microelectron. Eng.* 167 (2017) 69–79.
- [20] G. Zhang, Y. Cao, Y. Zhang, X. Song, J. Lu, S. Li, Preparation and characteristic analysis of ultra-low dielectric constant nano-porous silicon oxide films, *Advanced Graphic Communication, Printing and Packaging Technology: Proceedings of 2019 Tenth China Academic Conference on Printing and Packaging*, Springer, 2020, pp. 730–736.
- [21] J.I. Wang, M.A. Yamoah, Q. Li, A.H. Karamlou, T. Dinh, B. Kannan, J. Braumüller, D. Kim, A.J. Melville, S.E. Muschinske, Hexagonal boron nitride as a low-loss dielectric for superconducting quantum circuits and qubits, *Nat. Mater.* 21 (4) (2022) 398–403.
- [22] S. Hong, C.-S. Lee, M.-H. Lee, Y. Lee, K.Y. Ma, G. Kim, S.I. Yoon, K. Ihm, K.-J. Kim, T.J. Shin, Ultralow-dielectric-constant amorphous boron nitride, *Nature* 582 (7813) (2020) 511–514.
- [23] K. Zhang, L. Han, P. Froimowicz, H. Ishida, A smart latent catalyst containing o-trifluoroacetamide functional benzoxazine: precursor for low temperature formation of very high Performance polybenzoxazole with low dielectric constant and high thermal stability, *Macromolecules* 50 (17) (2017) 6552–6560.
- [24] L. Wang, X. Liu, C. Liu, X. Zhou, C. Liu, M. Cheng, R. Wei, X. Liu, Ultralow dielectric constant polyarylene ether nitrile foam with excellent mechanical properties, *Chem. Eng. J.* 384 (2020) 123231.
- [25] Y. Zhuang, J.G. Seong, Y.M. Lee, Polyimides containing aliphatic/alicyclic segments in the main chains, *Prog. Polym. Sci.* 92 (2019) 35–88.
- [26] J. Chen, M. Zeng, Z. Feng, T. Pang, Y. Huang, Q. Xu, Design and preparation of benzoxazine resin with high-frequency low dielectric constants and ultralow dielectric losses, *ACS Appl. Polym. Mater.* 1 (4) (2019) 625–630.
- [27] G. Lamoureux, G. Artavia, Use of the adamantane structure in medicinal chemistry, *Curr. Med. Chem.* 17 (26) (2010) 2967–2978.
- [28] Y. Zhang, Z. Geng, S. Niu, S. Zhang, J. Luan, G. Wang, Preparation and applications of low-dielectric constant poly aryl ether, *Adv. Ind. Eng. Polym. Res.* 3 (4) (2020) 175–185.
- [29] D.J. Liaw, B.Y. Liaw, J.J. Hsu, Y.C. Cheng, Synthesis and characterization of new soluble polyesters derived from various cardo bisphenols by solution polycondensation, *J. Polym. Sci. Part A Polym. Chem.* 38 (24) (2000) 4451–4456.
- [30] K. Wang, R. Yin, J. Nie, Q. Yu, Synthesis and characterization of a novel dimethacrylate based on adamantane as possible dental resins, *Mater. Sci. Eng. C* 32 (5) (2012) 1141–1145.

- [31] F. Zou, H. Chen, S. Fu, S. Chen, Shape memory materials based on adamantane-containing polyurethanes, *RSC Adv.* 8 (45) (2018) 25584–25591.
- [32] J. Ma, K. Cai, C. Yang, M. Li, X. Pan, Y. Huang, J. Yao, J. Zheng, J. Shao, Synthesis and properties of photocurable polyurethane acrylate for textile artificial leather, *Prog. Org. Coat.* 171 (2022) 107017.
- [33] M. Staffová, F. Ondreáš, J. Svatík, M. Zbončák, J. Jančář, P. Lepcio, 3D printing and post-curing optimization of photopolymerized structures: basic concepts and effective tools for improved thermomechanical properties, *Polym. Test.* 108 (2022) 107499.
- [34] J.-L. You, C.-P. Chang, N.-W. Pu, Y.-S. Chen, L.-H. Wang, K.-H. Pan, M.-D. Ger, Electroless plating of a 5G copper antenna on polyimide patterned with laser-induced selective activation and curing of metal–organic catalyst, *Appl. Surf. Sci.* 599 (2022) 153990.
- [35] J.-L. You, Y.-S. Chen, C.-P. Chang, M.-Z. Wu, M.-D. Ger, Utilizing a pH-responsive palladium nanocomposite to fabricate adhesion-enhanced and highly reliable copper coating on nylon 6 fabrics, *J. Mater. Res. Technol.* 15 (2021) 3983–3994.
- [36] J. Joseph, E.D. Jemmis, Red-, blue-, or no-shift in hydrogen bonds: a unified explanation, *J. Am. Chem. Soc.* 129 (15) (2007) 4620–4632.
- [37] Y. Meng, Y. Huang, C. Wang, L. Wang, Q. Fan, J. Shao, Tertiaryamine linked and polysiloxane modified polyurethane acrylate oligomer and its effects of migration/co-initiation on photo-curable inkjet printing, *Prog. Org. Coat.* 152 (2021) 106114.
- [38] Z. Wang, S.F. Zhou, Y.Z. Zhuo, A.N. Lai, Y.Z. Lu, X.B. Wu, Adamantane-based block poly (arylene ether sulfone) s as anion exchange membranes, *Polymer* 255 (2022) 125155.
- [39] Z. Geng, Y. Lu, S. Zhang, X. Jiang, P. Huo, J. Luan, G. Wang, Synthesis and characterization of novel adamantane-based copoly (aryl ether ketone) s with low dielectric constants, *Polym. Int.* 63 (2) (2014) 333–337.
- [40] C.-W. Tsai, J.-C. Wang, F.-N. Li, Y.-C. Chang, K.-H. Wu, Synthesis of adamantane-containing methacrylate polymers: characterization of thermal, mechanical, dielectric and optical properties, *Mater. Express* 6 (3) (2016) 220–228.
- [41] H.S. Huang, Y.C. Liao, Thermal and dielectric properties enhancement of photocurable acrylate polymers for digital light processing 3D printed electronics, *J. Appl. Polym. Sci.* 139 (18) (2022) 52070.
- [42] H. Xu, F. Qiu, Y. Wang, W. Wu, D. Yang, Q. Guo, UV-curable waterborne polyurethane-acrylate: preparation, characterization and properties, *Prog. Org. Coat.* 73 (1) (2012) 47–53.
- [43] C. Hong, X. Zhou, Y. Ye, W. Li, Synthesis and characterization of UV-curable waterborne Polyurethane–acrylate modified with hydroxyl-terminated polydimethylsiloxane: UV-cured film with excellent water resistance, *Prog. Org. Coat.* 156 (2021) 106251.
- [44] J. Huang, Y. Xiong, X. Zhou, Z. Yang, T. Yuan, A novel polyfunctional polyurethane acrylate prepolymer derived from bio-based polyols for UV-curable coatings applications, *Polym. Test.* 106 (2022) 107439.
- [45] T.S.R.T. Naiwi, M.M. Aung, M. Rayung, A. Ahmad, K.L. Chai, M.L.W. Fui, E.Z. M. Tarmizi, N.A.A. Aziz, Dielectric and ionic transport properties of bio-based polyurethane acrylate solid polymer electrolyte for application in electrochemical devices, *Polym. Test.* 106 (2022) 107459.
- [46] D. Zhang, J. Liu, Z. Li, Y. Shen, P. Wang, D. Wang, X. Wang, X. Hu, Preparation and properties of UV-curable waterborne silicon-containing polyurethane acrylate emulsion, *Prog. Org. Coat.* 160 (2021) 106503.
- [47] J. Miao, X. Hu, X. Wang, X. Meng, Z. Wang, J. Yan, Colorless polyimides derived from adamantane-containing diamines, *Polym. Chem.* 11 (37) (2020) 6009–6016.
- [48] T. Archibald, A. Malik, K. Baum, M. Unroe, Thermally stable acetylenic adamantane polymers, *Macromolecules* 24 (19) (1991) 5261–5265.
- [49] A. Galukhin, R. Nosov, G. Taimova, I. Nikolaev, D. Islamov, S. Vyazovkin, Polymerization kinetics of adamantane-based dicyanate ester and thermal properties of resulting polymer, *React. Funct. Polym.* 165 (2021) 104956.
- [50] G. Romero-Sabat, L.A. Granda, S. Medel, Synthesis of UV-curable polyurethane-acrylate hybrids with tuneable hardness and viscoelastic properties on-demand, *Mater. Adv.* 3 (12) (2022) 5118–5130.